Journal of Catalysis **195,** 244–252 (2000)
doi:10.1006/jcat.2000.3025, available online at http://www.idealibrary.com on IDEAL®

Alkali Effects on Molybdenum Oxide Catalysts for the Oxidative Dehydrogenation of Propane

Kaidong Chen, Shuibo Xie, Alexis T. Bell,[1] and Enrique Iglesia[1]

Chemical and Materials Sciences Divisions, E.O. Lawrence Berkeley National Laboratory, and Department of Chemical Engineering, University of California, Berkeley, California 94720-1462

Received February 1, 2000; revised August 8, 2000; accepted August 8, 2000

The effects of alkali oxides on the structure and on the catalytic behavior of MoO_x/ZrO_2 were examined for the oxidative dehydrogenation (ODH) of propane. X-ray diffraction, Raman and X-ray absorption spectroscopy, and estimates of the MoO_x surface density are consistent with the predominant presence of two-dimensional polymolybdate domains in samples with ~4 Mo/nm^2 surface density and $(alkali/Mo)_{at.}$ ratios of 0–0.2 treated in air at 773 K. The presence of alkali (Cs, K, Li) did not affect the structure of MoO_x domains, but influenced their electronic and catalytic properties. Propane ODH turnover rates decreased monotonically with increasing A : Mo atomic ratio and with increasing basicity of the alkali oxide (Cs > K > Li). These basic oxides inhibit the initial reduction of MoO_x in H_2 by strengthening Mo–O bonds and increasing reduction activation energies. As a result, rate-determining C–H bond activation steps, which involve the local reduction of Mo^{6+} centers, and the overall ODH catalytic sequence proceed more slowly when alkali oxides modify the MoO_x domains. The ratio of the rate constant for primary propane combustion (k_2) to that for propane ODH (k_1) is small (~0.1) and it increased slightly with increased alkali content. The ratio of the propene combustion rate constant (k_3) to the propane ODH rate constant (k_1) is large (15–25); it decreased with the addition of small amounts of alkali (alkali/Mo ~ 0.05) and then remained constant at higher alkali contents. The stronger inhibition of secondary propene combustion reactions relative to that of primary ODH steps reflects the weaker Lewis acidity of Mo^{6+} cations modified by the strongly basic alkali oxide species. These effects decrease the binding energy of propene on the sites required for C–H bond activation of both propene and propane. They also account for the lower reaction rates and for the higher selectivity observed at a given propane conversion on alkali-modified MoO_x ODH catalysts.

INTRODUCTION

The oxidative dehydrogenation (ODH) of light alkanes provides a potential low-temperature route for the synthesis of alkenes (1–5), but its current practice is limited by a marked decrease in propene selectivity with increasing conversion (2, 3), which leads to propene yields lower than 30% (3). Most oxidative dehydrogenation catalysts contain V or Mo oxides as the active component (3). Recent reports have suggested that the addition of basic oxides increases propene selectivity on these catalysts (6–8), but the concurrent decrease in ODH rates leads to lower conversion, which can give the appearance of more selective catalysts by merely minimizing secondary combustion reactions. The addition of alkali oxides to Mo-based catalysts changes the electronic properties of the MoO_x active phase (9). Changes in the catalyst structure can also occur; for example, new phases, such as alkali molybdates, can form at high alkali/Mo ratios as a result of strong interactions between acidic MoO_3 and basic alkali oxides (10).

The oxidation of propane to propene occurs via parallel and sequential oxidation steps (Scheme 1) (1). Propene forms via primary reactions limited by initial C–H bond activation elementary steps (k_1), while CO and CO_2 (CO_x) can form via either secondary propene combustion (k_3) or primary propane combustion (k_2). The k_2/k_1 ratio (primary propane combustion/primary propane dehydrogenation) is generally low (~0.1) for selective ODH catalysts (11–13). The yield losses with increasing conversion reflect the large values of k_3/k_1 (propene secondary combustion/propane primary dehydrogenation) ratios (~10–50), which arise from the weaker C–H bonds in propene compared with those in propane, as well as from the higher binding energy of alkenes on oxide surfaces (11–13). Since propene selectivities at moderate conversions depend on both k_2/k_1 and k_3/k_1, it is unclear whether any yield changes caused by alkali addition arise from their effect on primary or secondary combustion steps. Here, we examine the effects of alkali modifications of ZrO_2-supported polymolybdate domains (13) by measuring individual rate constants and their ratios as a function of the identity and concentration of the alkali species. The effects of alkali on the structure and reducibility of the MoO_x domains were examined by *in situ* Raman and X-ray absorption methods and by kinetic studies of the initial reduction of MoO_x domains in H_2.

[1] Authors to whom correspondence should be addressed. E-mail: iglesia@cchem.berkeley.edu; bell@cchem.berkeley.edu.

0021-9517/00 $35.00

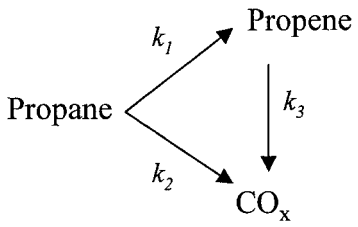

SCHEME 1. Reaction network in oxidative dehydrogenation of propane reactions.

EXPERIMENTAL

Zirconium oxyhydroxide ($ZrO(OH)_2$) was prepared by precipitation from a zirconyl chloride solution (98%, Aldrich, Inc.) at a pH of 10, maintained constant by controlling the rate of addition of an ammonium hydroxide solution (29.8%, Fischer Scientific, Inc.). The precipitated solids were washed with mildly basic ammonium hydroxide solution (pH $\sim$ 8) until the effluent showed no chloride ions by a silver nitrate test and then dried in air overnight at 393 K.

ZrO_2-supported MoO_x samples were modified with alkali using incipient wetness coimpregnation of precipitated zirconium oxyhydroxide powders with a solution containing ammonium dimolybdate (ABM) (99%, Aldrich, Inc.) and the alkali nitrate salt (99.9%, Aldrich, Inc.). Alkali-modified samples are denoted as *n*A–Mo/Zr, where A denotes the alkali metal used and *n* is the A : Mo atomic ratio. Impregnated samples were dried overnight in air at 393 K and then treated in dry air (Airgas, zero grade) at 773 K for 3 h. Their nominal MoO_3 concentration is 11 wt%. Alkali/Mo atomic ratios were kept below 0.2 in order to avoid the formation of bulk-phase alkali molybdates. The MoO_x/ZrO_2 catalyst without alkali is identified as Mo/Zr.

Surface areas were measured by N_2 physisorption using a Quantasorb apparatus (Quantachrome Corporation) and standard multipoint BET analysis methods. Samples were vacuated for 3 h at 383 K before N_2 (Airgas, 99.999%) physisorption measurements. Powder X-ray diffraction patterns were obtained at room temperature using a Siemens diffractometer and Cu $K\alpha$ radiation and a small catalyst sample mixed with Vaseline and spread on a thin glass plate.

Raman spectra were obtained using a HoloLab Series 5000 Raman spectrometer (Kaiser Optical) equipped with an Nd YAG laser that is frequency-doubled to 532 nm. Samples ($\sim$50 mg) were pressed into wafers at 350 MPa pressure (0.9 cm diameter, 0.1 cm thickness) and placed within a quartz cell (11). The laser was operated at a power level of 75 mW. The sample stage was rotated at 20 Hz in order to reduce the effect of laser heating on the local sample temperature. Raman spectra of hydrated samples were recorded at ambient conditions. Samples were dehydrated at 673 K in 20% O_2/He for 1 h and then cooled to room temperature in the same atmosphere before measurement of Raman spectra.

Mo *K*-edge X-ray absorption spectra (XAS) were measured using beamline 4-1 at the Stanford Synchrotron Radiation Laboratory (SSRL) using an *in situ* cell (14). All samples were diluted with SiO_2 to about 5 wt% MoO_3, pressed into wafers, crushed, and sieved to retain particles with 0.18–0.25 mm diameter. These particles were placed within thin quartz capillaries (1.0 mm diameter, 0.1 mm wall thickness) and supported horizontally in the path of the rectangular X-ray beam (0.2 mm $\times$ 6.0 mm). Spectra were measured in transmission mode with Ar gas in three ion chamber detectors: one located before the sample to measure the incident X-ray intensity (I_0), one located after the sample and before a Mo foil (7.5 μm) to measure the intensity after the sample (I_1), and one placed after the Mo foil in order to measure the beam intensity after the Mo foil (I_2). The sample spectrum and the Mo foil spectrum are reported as $\log(I_0/I_1)$ and $\log(I_1/I_2)$, respectively. The energy was calibrated using the first inflection point in the Mo foil spectrum (19.999 keV). Spectra were measured using a Si(220) crystal monochromator with 5-eV energy increments in the pre-edge region (19.875 to 19.975 keV), 0.25-eV increments in the edge region (19.975 to 20.035 keV), and 0.04 $Å^{-1}$ in the fine structure region (20.035 to 21.024 keV). X-ray absorption data were analyzed using WinXAS software (version 1.2) (15). A linear fit to the pre-edge region was subtracted from the entire spectrum, and then the spectrum was normalized using a fifth-order polynomial fit to the post-edge fine structure (EXAFS) region. The XANES region of the spectra was analyzed between 19.900 keV and 20.150 keV using principal component analysis (15).

Temperature-programmed reduction studies were carried out using a Quantasorb surface area analyzer (Quantachrome Corporation) modified with electronic mass flow meters, a programmable furnace, and on-line 13$\times$ molecular sieve traps in order to remove the water formed during reduction before thermal conductivity measurements. A 20% H_2/Ar mixture (Matheson UHP, certified mixture) flowing at 1.33 $cm^3\,s^{-1}$ was used to reduce samples ($\sim$0.2 g) held within a 4-mm-i.d. quartz cell containing a quartz thermowell directly in contact with the sample bed. Reduction rates were obtained by thermal conductivity measurements of the H_2 concentration in the exit stream as the sample temperature was increased from room temperature to 1250 K at 0.167 K s^{-1}. The thermal conductivity response was calibrated using the complete reduction of CuO powder (Aldrich, 99.995%).

ODH selectivity and rate measurements were carried out in a packed-bed tubular quartz reactor using 0.03- to 0.3-g catalyst samples at 703 K. Propane (Airgas, 99.9%) and oxygen (Airgas, 99.999%) at 14.03 kPa and 1.74 kPa, respectively, were used as reactants and He (Airgas, 99.999%) was used as a diluent. On-line analysis of reactants and products was performed by gas chromatography (Hewlett-Packard 5880 GC) using procedures described in detail elsewhere

(11, 12). C_3H_8 and O_2 conversions were varied by changing reactant space velocity (F/w, where w is the mass of catalyst and F is the propane flow rate in cm^3/s). Typical conversions were below 2% for C_3H_8 and below 20% for O_2. All reported ODH reaction rates and selectivities were extrapolated to zero residence time in order to determine rates and rate constants for primary ODH and combustion reactions. The effect of bed residence time on product yields was used in order to calculate rates and rate constants for secondary propene combustion reactions, using procedures reported previously (11–13).

RESULTS AND DISCUSSION

The crystal structures of ZrO_2, Mo/Zr, and A–Mo/Zr samples were examined by X-ray diffraction (Fig. 1). Diffraction peaks assigned to both tetragonal and monoclinic phases of zirconia were detected in the pure ZrO_2 samples. The presence of MoO_x (11 wt%) on the ZrO_2 surface inhibits the formation of the monoclinic ZrO_2 phase and leads to the formation of pure tetragonal ZrO_2 after treatment in air at 773 K for 3 h (Fig. 1). These tetragonal stabilization effects are similar to those reported previously for VO_x/ZrO_2 (11) and WO_x/ZrO_2 (16). At this treatment temperature, no crystalline MoO_3 or $ZrMO_2O_8$ phases are formed and MoO_x domains appear to be well dispersed on the ZrO_2 surface, as indicated by the absence of diffraction peaks for MoO_x species. The diffraction patterns for Cs-doped Cs–Mo/Zr samples with different Cs : Mo atomic ratios resemble those for the alkali-free Mo/Zr sample. Only tetragonal ZrO_2 peaks are present in the diffraction pattern. Thus, no significant structural effects of alkali were detected by X-ray diffraction in these samples. These results, however, do not rule out that the local structure of the predominant dispersed polymolybdate domains can be influenced by alkali, because X-ray diffraction detects only crystalline structures with domain sizes larger than 2–5 nm.

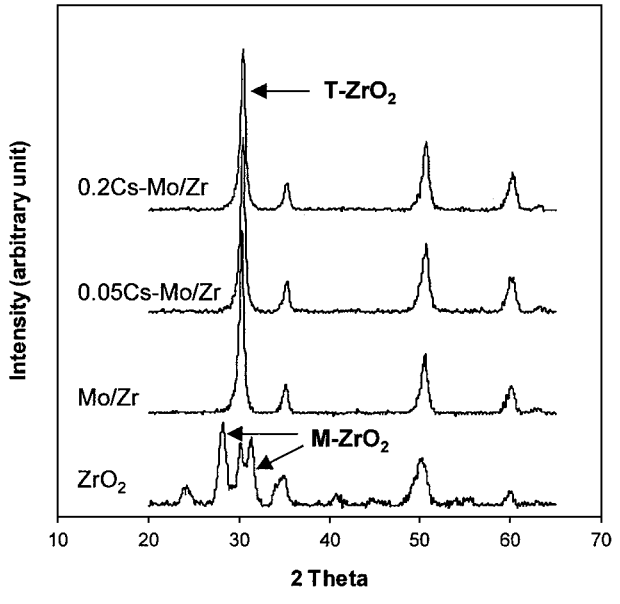

FIG. 1. X-ray diffraction patterns of ZrO_2, Mo/Zr, and A–Mo/Zr catalysts.

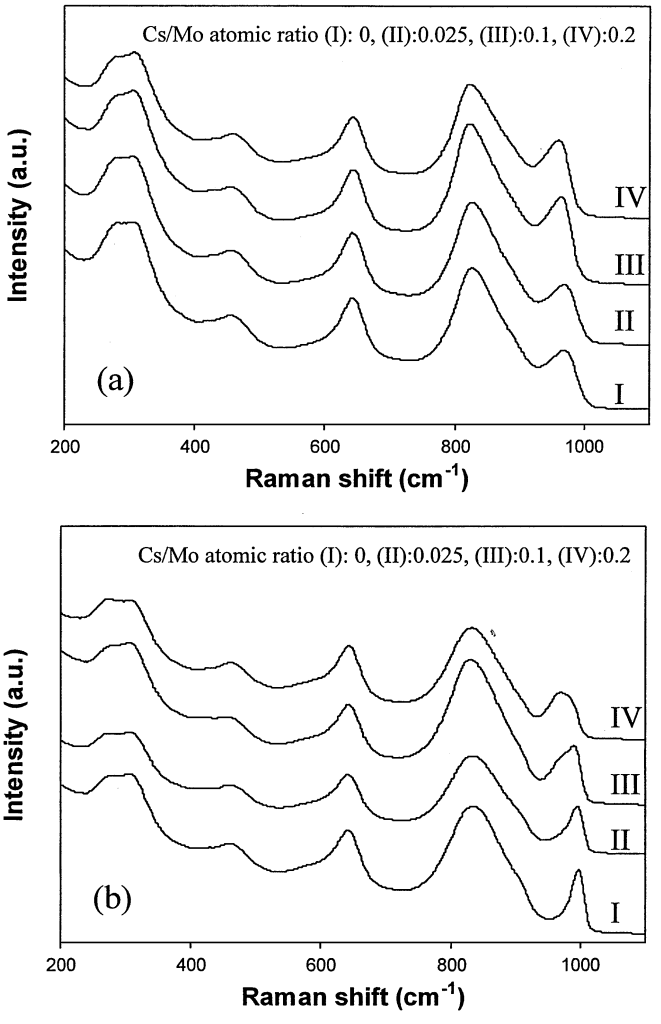

FIG. 2. Raman Spectra of Mo/Zr and A–Mo/Zr catalysts: (a) hydrated and (b) dehydrated.

Raman spectroscopy can detect changes in local structure by probing the metal–oxygen vibrational modes of metal oxides. Raman spectra for hydrated and dehydrated Mo/Zr and Cs–Mo/Zr samples with different Cs : Mo atomic ratios are shown in Figs. 2a and 2b, respectively. The Raman spectra for all the hydrated samples are very similar (Fig. 2a). The Raman band at ~829 cm^{-1} corresponds to Mo–O–Mo vibrations (17, 18) and the band at ~970 cm^{-1} is assigned to Mo=O vibrations (17–20) in two-dimensional polymolybdates. No bands at 998 cm^{-1}, corresponding to crystalline MoO_3, were observed in any of the samples. These results are consistent with the X-ray diffraction results and they suggest that MoO_x domains exist as two-dimensional polymolybdate structures. Figure 2b shows the Raman spectra

of dehydrated samples. Compared with the spectra of hydrated samples (Fig. 2a), the bands at ~970 cm^{-1} shift to higher wavenumbers upon dehydration (18); the band shape also changes and becomes broader and more asymmetric with increasing Cs/Mo atomic ratio. These results suggest that the addition of a small amount of alkali does not influence the dispersion state of MoO_x species, but it affects the electronic properties of MoO_x domains. Raman bands detected at 280, 316, 467, and 647 cm^{-1} can be assigned to tetragonal ZrO_2 (21), which was also detected by X-ray diffraction.

The Mo *K*-near-edge spectra for MoO_3, ammonium dimolybdate, Mo/Zr, and Cs–Mo/Zr samples are shown in Fig. 3a. Figure 3b shows the difference spectra for each sample relative to the alkali-free Mo/Zr spectrum. The Mo *K*-edge detected at ~20 keV corresponds to the ejection of a Mo 1*s* electron, while the pre-edge feature at ~19.99 keV arises from a 1*s* to 4*d* electronic transition that is dipole-forbidden in centrosymmetric structures. Mo^{6+} centers in MoO_3 occupy off-center positions in MoO_6 octahedra and this distortion allows these forbidden transitions to occur. The intensity of this pre-edge feature increases as the Mo^{6+} centers acquire tetrahedral symmetry, as a result of greater *p–d* orbital mixing (22).

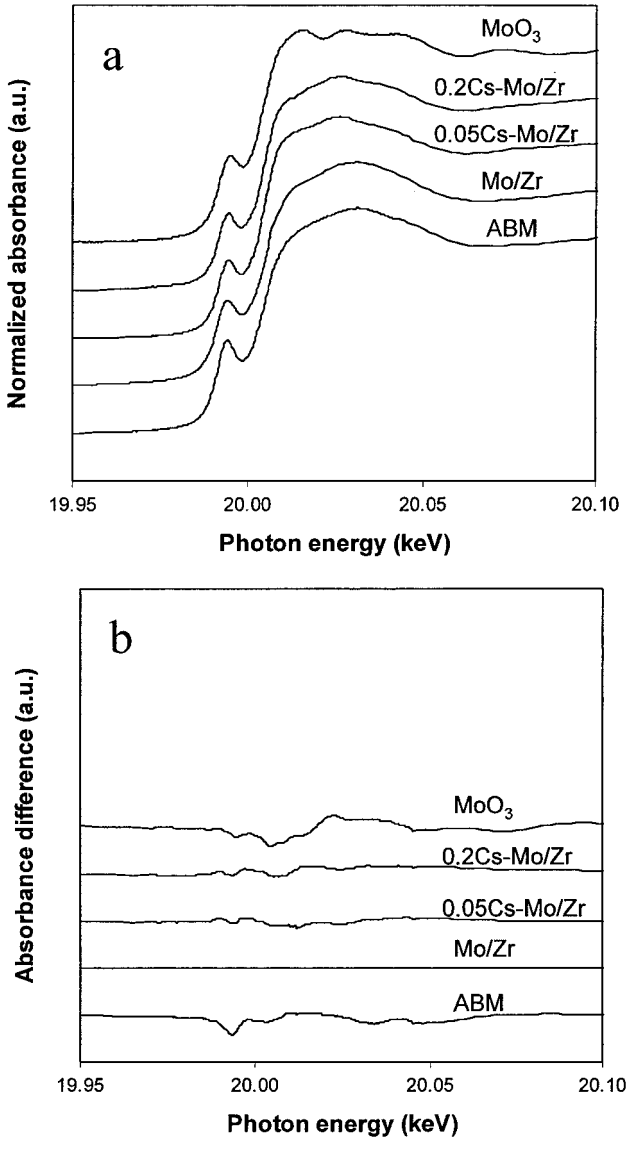

FIG. 3. (a) Near-edge X-ray absorption spectra of ammonium bimolybdate (ABM), Mo/Zr, A–Mo/Zr, and MoO_3 samples, and (b) difference spectra obtained by using Mo/Zr sample as reference.

TABLE 1

Surface Area and Mo Surface Density of Mo/Zr and A–Mo/Zr Catalysts

Catalyst	Surface area (m^2/g)	Mo surface density (Mo/nm^2)
Mo/Zr	133	3.5
0.025Cs–Mo/Zr	118	3.9
0.05Li–Mo/Zr	130	3.5
0.05K–Mo/Zr	143	3.2
0.05Cs–Mo/Zr	117	3.9
0.1Cs–Mo/Zr	115	4.0
0.2Cs–Mo/Zr	105	4.4

Near-edge X-ray absorption spectra can be used to probe changes in local structure and electronic properties by comparing them with the near-edge features in relevant reference compounds (23–25). The near-edge spectra of Mo/Zr and Cs–Mo/Zr samples resemble more closely the spectrum of ammonium dimolybdate than that of crystalline MoO_3, consistent with the proposed dispersed nature of MoO_x domains in these samples. The near-edge spectra for Cs–Mo/Zr and Mo/Zr samples are similar, but small differences are clearly observed (Fig. 3b). This suggests that the MoO_x structures in these catalysts are similar, but that alkali influences the electronic properties of MoO_x species, as also concluded from the Raman spectra.

Geometric arguments and structural characterization of dispersed MoO_x species on ZrO_2 show that polymolybdate layers formed after treatment in air at 773 K for surface densities below 5 Mo/nm^2 (17, 26–28). The Mo surface densities calculated from the measured BET surface areas are shown in Table 1 for all Mo/Zr and A–Mo/Zr samples. Mo surface densities are reported as Mo atoms per nm^2. Since alkali additives do not strongly influence the surface area of MoO_x/ZrO_2 samples, Mo surface densities are similar for all samples (3.2–4.4 Mo/nm^2) and the values are lower than those reported for complete coverage of the surface with a polymolybdate monolayer (~5 Mo/nm^2). This is consistent with the conclusions from X-ray diffraction, Raman, and X-ray absorption data that surface MoO_x species are present as two-dimensional polymolybdate domains.

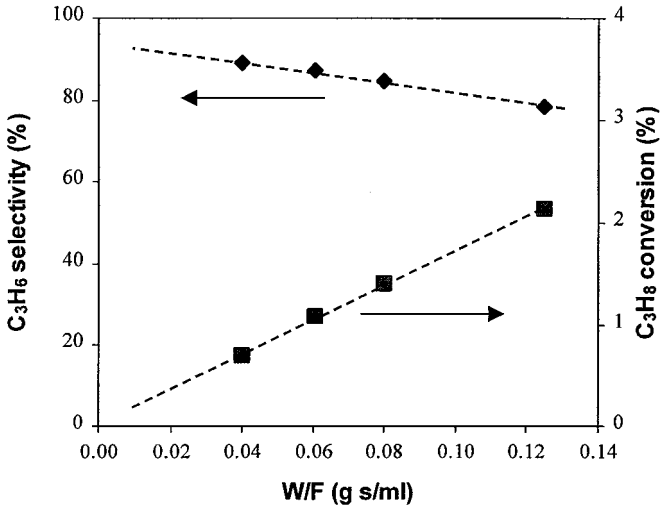

FIG. 4. Dependence of propane conversion and propene selectivity on bed residence time (Mo/Zr, 703 K, 14 kPa C_3H_8, 1.7 kPa O_2, balance He).

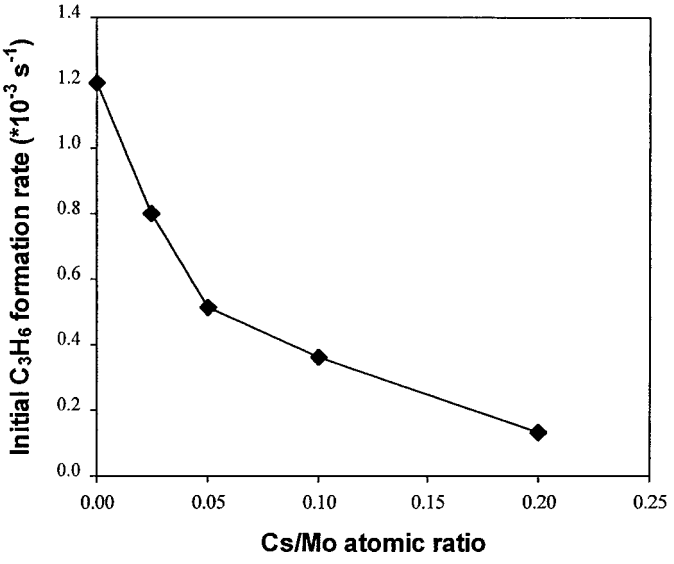

FIG. 5. Dependence of initial propene formation rate on Cs : Mo atomic ratio for Cs–Mo/Zr samples (703 K, 14 kPa C_3H_8, 1.7 kPa O_2, balance He).

Catalytic data on all Mo/Zr and A–Mo/Zr samples are reported in Figs. 4–7 and Figs. 12 and 13. Figure 4 shows the values of propane conversion and propene selectivity obtained as a function of reactor residence time on the alkali-free Mo/Zr sample. Propene selectivities decreased as the propane conversion increased with increasing reactor residence time, as expected from the greater contribution of secondary propene combustion reactions to the observed products. The reaction rate constants k_1, k_2, and k_3 can be calculated for each sample from data similar to those in Fig. 4 using the reaction sequence shown in Scheme 1 (11). At the modest H_2O concentrations prevalent at the low conversions of these experiments, the rate of each reaction can be described accurately by

$$r_1 = k_1[C_3H_8] \quad [1]$$

$$r_2 = k_2[C_3H_8] \quad [2]$$

$$r_3 = k_3[C_3H_6], \quad [3]$$

where k_i is the apparent first-order rate coefficient for reaction i. The propene selectivity at relatively low conversions for the plug-flow hydrodynamics of the reactor used are accurately described by

$$S = S^0[1 - (k_3C_v/2)\tau], \quad [4]$$

where C_v is the concentration of Mo atoms per unit reactor volume, τ is the reactor residence time, and $S^0 = k_1/(k_1 + k_2)$ is the initial propene selectivity (at zero conversion). The value of k_1 can be obtained from the initial rate of propene conversion (as $\tau \to 0$) and the value of k_2 from the initial propene selectivity (S^0). The value of k_3 can then be obtained from the dependence of propene selectivity on reactor residence time, as described by Eq. [4].

Initial propane ODH reaction rates (normalized by the total number of Mo atoms) are reported in Figs. 5 and 6 as a function of alkali identity and content. The addition of Cs to Mo/Zr catalysts markedly decreased propane ODH turnover rates; these effects become stronger as the Cs content increases (Fig. 5). At a given alkali/Mo atomic ratio (A : Mo = 0.05), propane ODH turnover rates decreased in

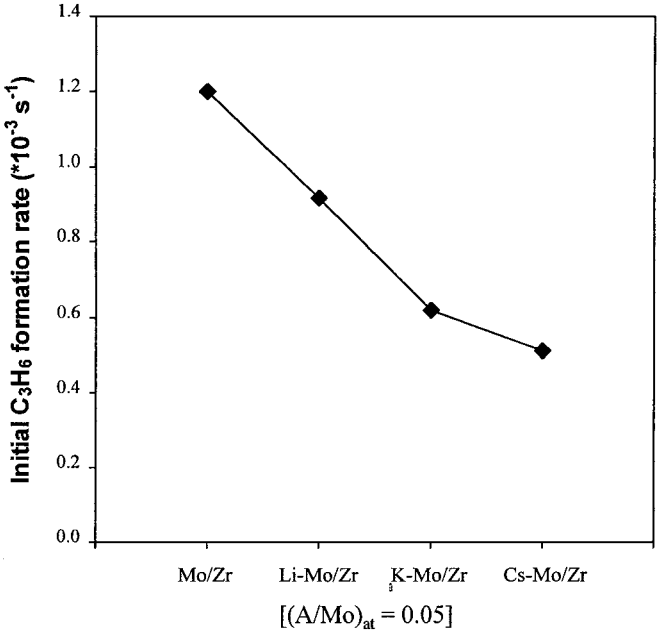

FIG. 6. Dependence of initial propene formation rate on different alkali additives for 0.05A–Mo/Zr samples (703 K, 14 kPa C_3H_8, 1.7 kPa O_2, balance He).

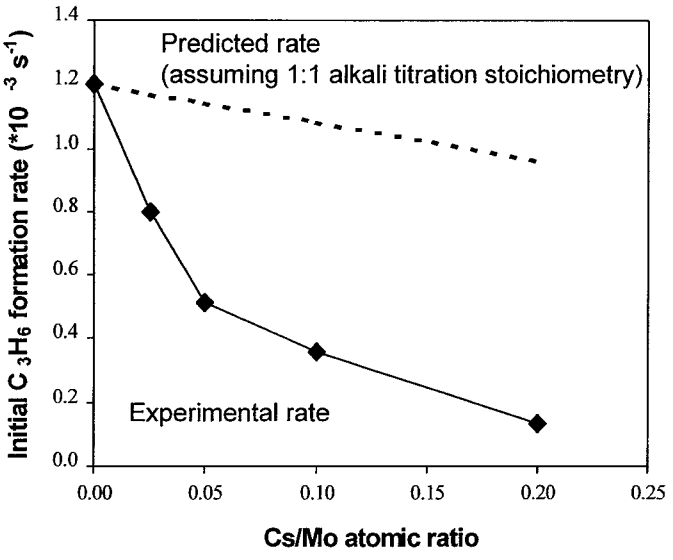

FIG. 7. Comparison of experimental and predicted (from 1 : 1 site titration stoichiometry) initial propene formation rate on Cs–Mo/Zr samples with different Cs : Mo atomic ratio (703 K, 14 kPa C_3H_8, 1.7 kPa O_2, balance He).

the order Li–Mo/Zr > K–Mo/Zr > Cs–Mo/Zr (Fig. 6), suggesting that the reaction rate inhibition effects increase with increasing basicity of the alkali metal oxide species. The observed rate inhibition and the trends with increasing alkali oxide basicity are consistent with those reported in the literature for alkali-modified $MoO_x/MgO–Al_2O_3$ (6), VO_x/ZrO_2 (7), MoO_x/TiO_2, and VO_x/TiO_2 (8).

Since all of the Mo/Zr and A–Mo/Zr catalysts in this study consist of two-dimensional polymolybdate domains, most of the Mo atoms in the catalysts are accessible at the surface and available for propane conversion reactions. Alkali species (oxides, hydroxides, or carbonates) can block some MoO_x active sites and make such sites inaccessible, but the fraction of such covered sites is unlikely to exceed the A : Mo atomic ratio (<0.2). Figure 7 shows the measured rates and those calculated if each alkali ion is assumed to block only one Mo site. Measured rates were much lower than expected from the titration of one Mo site by each alkali cation. It is possible that some exposed MoO_x species are especially active in ODH reactions and that these sites are also preferentially titrated by alkali, but experimental evidence for such nonuniform site distributions has not been reported. Since alkali inhibition effects depend on the basicity of alkali oxides (Fig. 6), alkali effects reflect not only the blocking of Mo sites by alkali species, but also changes in the electronic properties of MoO_x domains as shown by Raman and X-ray absorption studies. Such electronic modification can extend to a significant number of neighboring MoO_x sites because of the significant electronic conductivity of semiconducting oxides (9).

Recent kinetic studies have confirmed the proposal that C–H bond activation steps using lattice oxygen limit the rate of propane ODH reactions on V- and Mo-based catalysts (29, 30). C–H bond dissociation steps involve the incipient reduction of the metal cations; as a result, the required activation barrier depends on the reducibility of the metal oxide catalyst (30). For V- and Mo-based catalysts, propane ODH reaction rates decrease as the reducibility of the metal cations decreases (6–8, 30). The kinetics of MoO_x reduction in H_2 can be probed using temperature-programmed reduction (TPR) methods. Figure 8 shows TPR profiles for Mo/Zr and Cs–Mo/Zr catalysts. The general features are similar in all the samples. Two broad peaks are detected below 1273 K; the low-temperature peak (~700 K) corresponds to the reduction of Mo^{6+} to Mo^{4+} and the high-temperature peak reflects the reduction of Mo^{4+} to Mo^0 (31). The temperature of both reduction peaks increased with increasing Cs : Mo atomic ratio, suggesting that the reduction of MoO_x is more difficult for Cs-containing samples.

The reducibility of MoO_x species was also examined by *in situ* X-ray absorption measurements during treatment in H_2. Before the spectra were measured, a flow of 20% H_2/Ar was passed over the sample for 20 min at room temperature, and then the sample temperature was increased (at 0.167 K s^{-1}) to a specified temperature and then quickly cooled to room temperature in H_2/Ar flow. All X-ray absorption spectra were measured at room temperature. Figure 9 shows the spectra for 0.2Cs–Mo/Zr after exposure to the reduction mixture at RT, 673 K, 773 K, and 873 K. Figure 9 also shows a MoO_2 reference spectrum. It is seen that the spectrum of 0.2Cs–Mo/Zr gradually changes and becomes to similar to that of MoO_2 after higher temperature reduction. Below 873 K, Mo^{6+} and Mo^{4+} ions coexist in the sample and the near-edge spectrum represents the overlap of the spectra for these two species. The relative concentration of Mo^{6+} and Mo^{4+} ions can be obtained by describing the composite spectra as a linear combination of

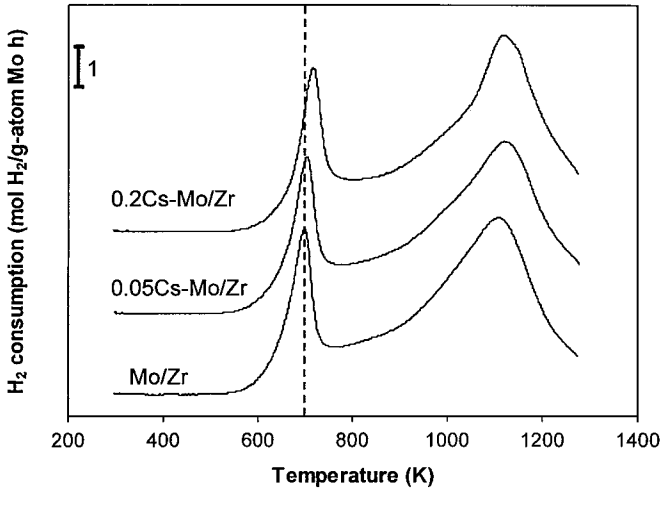

FIG. 8. Temperature-programmed reduction profiles of Mo/Zr and Cs–Mo/Zr samples.

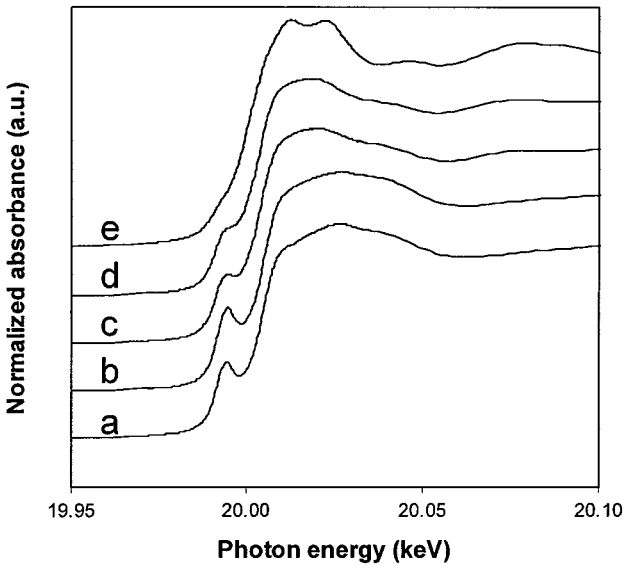

FIG. 9. Near-edge X-ray absorption spectra of 0.2Cs–Mo/Zr sample (a) Under ambient conditions, (b) after reduction in H_2 to 673 K, (c) after reduction in H_2 to 773 K, and (d) after reduction in H_2 to 873 K; (e) MoO_2 reference compound.

the initial sample spectrum (at RT) and of the spectrum of MoO_2 (15). Figure 10 shows the fraction of MoO_2 obtained by this method for Mo/Zr and 0.2Cs–Mo/Zr samples after reduction at 673 K, 773 K, and 873 K. Clearly, the amount of Mo^{4+} formed in 0.2Cs–Mo/Zr is significantly lower than in Mo/Zr, confirming that the addition of Cs inhibits the reduction of MoO_x domains supported on ZrO_2.

The kinetics of ODH on MoO_x/ZrO_2 show that the catalytic surface is predominately covered with oxide anions and vacancies are minority surface species (30). Therefore, it appears that the first reduction peak in the TPR profile,

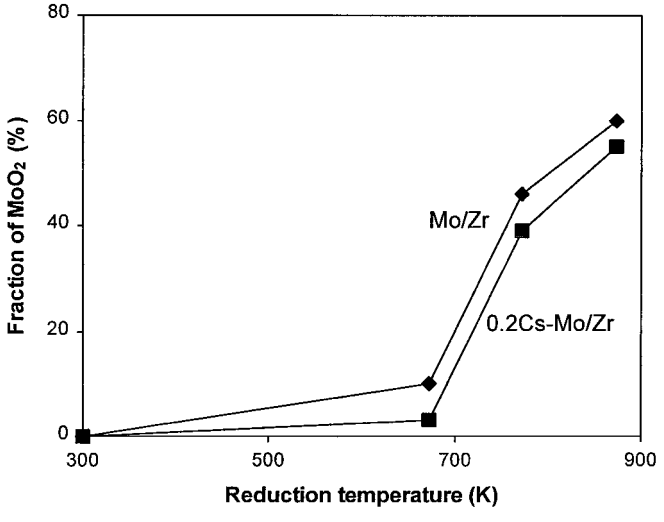

FIG. 10. Fraction of MoO_2 calculated from XANES fit in Mo/Zr and 0.2Cs–Mo/Zr samples after reduction in H_2 at different temperatures.

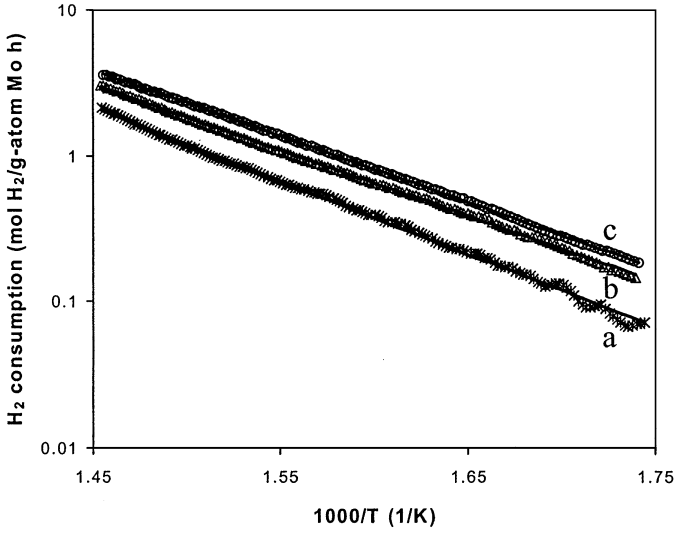

FIG. 11. H_2 reduction rate as a function of temperature for (a) 0.2Cs–Mo/Zr, (b) 0.05Cs–Mo/Zr, and (c) Mo/Zr samples.

and specifically the initial stages of this reduction peak, represents the reduction processes most relevant to the ODH reaction. Figure 11 shows the rate of reduction of Mo^{6+} to Mo^{4+} by H_2 as a function of temperature during the early stages of the Mo^{6+} reduction to Mo^{4+}. The reduction activation energies can be calculated on the basis of these data. At a given temperature, the reduction rate decreases with increasing Cs/Mo atomic ratio. The reduction activation energy for the 0.2Cs–Mo/Zr sample (96 kJ/mol) is higher than that for the Mo/Zr sample (86 kJ/mol). The results of these reduction studies suggest that the addition of alkali decreases the rate of reduction of the MoO_x species. Higher amounts of alkali or stronger basicity of the additive leads to lower MoO_x reduction rates, and also to lower propane ODH turnover rates. Similar results and correlations between reducibility and ODH reaction rates have been reported previously (6–8).

As shown in Fig. 4, propene selectivity decreased with increasing propane conversion because of secondary propene combustion reactions. Propene yields in propane ODH reactions depend on both k_2/k_1 and k_3/k_1, and smaller values of either ratio lead to higher propene selectivity at a given propane conversion. Figures 12 and 13 show the effect of alkali additives on k_2/k_1 and k_3/k_1, respectively. The k_2/k_1 ratio reflects the relative rates of primary C_3H_8 combustion and ODH reactions. Values of k_2/k_1 ratios are very small on all catalysts and they increase very slightly with increasing Cs : Mo atomic ratio (Fig. 12). Therefore, reactions of propane favor oxidative dehydrogenation over direct propane combustion reactions and the effect of Cs on the relative rates of these two reactions is small. The slight increase of k_2/k_1 ratios with increasing Cs content may reflect the stronger basicity of the lattice oxygen atoms, which can lead to stronger binding of propyl intermediates and to

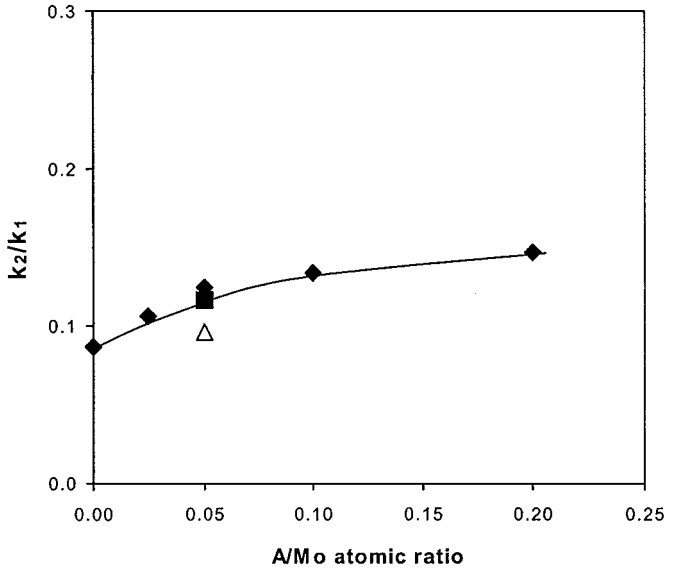

FIG. 12. Dependence of k_2/k_1 values on A : Mo atomic ratio for Mo/Zr and A–Mo/Zr samples: (◆) Cs–Mo/Zr, (■) Li–Mo/Zr, and (△) K–Mo/Zr (703 K, 14 kPa C_3H_8, 1.7 kPa O_2, balance He).

their undesired combustion before desorption as propene. These results appear to contradict previous reports by Sloczynski *et al.* (32) that addition of alkali (Rb) to V_2O_5/TiO_2 ODH catalysts decreases k_2/k_1 ratios. These alkali effects, however, were obtained from a nonrigorous comparison of catalysts at different temperatures and using a kinetic analysis that disproportionately considers higher conversion data in the fitting of initial dehydrogenation (k_1) and combustion (k_2) rates. Therefore, alkali effects on propene selectivities or yields mainly reflect changes in the much larger k_3/k_1 ratios with addition of Cs. Values of k_3/k_1 ratios are much greater than unity on all catalysts (Fig. 13) and they decrease with the addition of alkali. These effects of alkali on k_3/k_1 ratios account for the observed increase in propene selectivity at a given conversion on alkali-doped samples. The k_3/k_1 ratios, however, are almost independent of the A : Mo atomic ratio and of the different basicity of alkali additives for A : Mo atomic ratios greater than 0.05.

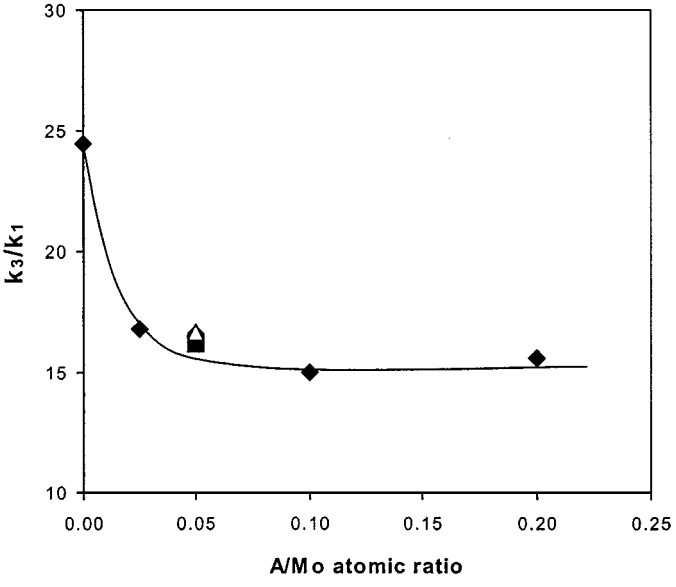

FIG. 13. Dependence of k_3/k_1 values on A : Mo atomic ratio for Mo/Zr and A–Mo/Zr samples: (◆) Cs–Mo/Zr, (■) Li–Mo/Zr, and (△) K–Mo/Zr (703 K, 14 kPa C_3H_8, 1.7 kPa O_2, balance He).

Our recent studies have shown that the k_3/k_1 ratio is strongly influenced by the $\Delta(\Delta H^{ads})$ value, which is the difference between the adsorption enthalpies for the molecular adsorption of propane (ΔH_1^{ads}) and of propene (ΔH_3^{ads}) on a given catalyst surface [$\Delta(\Delta H^{ads}) = \Delta H_1^{ads} - \Delta H_3^{ads}$]; the k_3/k_1 ratios decrease with decreasing $\Delta(\Delta H^{ads})$ values (30). $\Delta(\Delta H^{ads})$ depends strongly on the acid–base properties of MoO_x binding sites. Adsorption processes are exothermic and stronger molecule–site interactions lead to more negative adsorption enthalpies. Propene molecules contain a π-bond, which makes them more basic than propane; this leads to stronger interactions with electron-deficient Lewis centers on oxide surfaces than for propane. As a result, propene interacts more strongly than propane with oxides containing Lewis acid centers, and $\Delta(\Delta H^{ads})$ is always positive. $\Delta(\Delta H^{ads})$ decreases with decreasing Lewis acidity, and as a result, k_3/k_1 would also decrease. In supported MoO_x catalysts, Mo^{6+} ions act as Lewis acid sites. The addition of strongly basic alkali additives leads to electron transfer from the basic oxygen in the alkali oxide to the Mo^{6+} cation, which becomes less acidic and shows smaller $\Delta(\Delta H^{ads})$ values and smaller k_3/k_1 ratios. As the Lewis acid strength of Mo^{6+} cations decreases, however, the value of $\Delta(\Delta H^{ads})$ may become independent of acid strength and k_3/k_1 is not affected by higher alkali concentrations. This decrease in k_3/k_1 causes the observed higher propene selectivity on alkali-modified MoO_x catalysts.

CONCLUSIONS

MoO_x species exist predominately as two-dimensional polymolybdate domains in MoO_x/ZrO_2 samples with 4 Mo/nm^2 surface densities treated in air at 773 K. The addition of alkali at A : Mo atomic ratios below 0.2 does not influence the structure of the MoO_x domains or lead to the formation of any alkali-containing bulk Mo oxide phases. Raman and X-ray absorption, however, detect electronic modifications of the Mo^{6+} center upon addition of alkali (Cs, K, Li). Alkali addition decreases propane ODH reaction rates on MoO_x/ZrO_2 and the effects are stronger as the amount or the basicity of the alkali additive increases. Alkali effects also decrease the reducibility of MoO_x species in H_2. Alkali decreases the rate and increases the activation energy for the initial reduction of MoO_x/ZrO_2 samples in H_2.

The Mo^{6+} local reduction required for C–H bond activation rate-determining ODH steps appears to be inhibited also by the addition of alkali. The ODH k_2/k_1 ratio is very small ($\sim$0.1) for all samples and it increases slightly with increasing A : Mo atomic ratio. The ODH k_3/k_1 ratios are much larger than unity and they are primarily responsible for the low propene selectivity as conversion increases. The values of k_3/k_1 ratios decrease with the initial addition of alkali up to $(A/M)_{at.}$ values of 0.05 and remain constant for higher alkali concentrations. These selectivity enhancements apparently arise from alkali oxide effects on the electron density and Lewis acidity of the Mo^{6+} centers, which decrease the heat of adsorption of propene on the sites required for C–H bond activation in both propane and propene. The predominant effect of alkali on propene selectivity arises from its effect on the relative rates of secondary propene combustion and primary propane ODH reactions.

ACKNOWLEDGMENTS

This work was supported by the Director, Office of Basic Energy Sciences, Chemical Sciences Division of the U.S. Department of Energy under Contract DE-AC03-76SF00098. X-ray absorption data were collected at the Stanford Synchrotron Radiation Laboratory (SSRL), which is operated by the Department of Energy (DOE), Office of Basic Energy Sciences under contract DE-AC03-76SF00515. The authors acknowledge Dr. George Meitzner for help with the acquisition and analysis of the X-ray absorption data.

REFERENCES

1. Blasko, T., and López Nieto, J. M., *Appl. Catal. A* **157**, 117 (1997).
2. Kung, H. H., *Adv. Catal.* **40**, 1 (1994).
3. Albonetti, S., Cavani, F., and Trifiro, F., *Catal. Rev.—Sci. Eng.* **38**, 413 (1996).
4. Centi, G., and Triffiro, F., *Appl. Catal. A* **143**, 3 (1996).
5. Mamedov, E. A., and Cortés-Corberan, V., *Appl. Catal. A* **127**, 1 (1995).
6. Abello, M. C., Gomez, M. F., and Cadus, L. E., *Catal. Lett.* **53**, 185 (1998).
7. Albrecht, S., Wendt, G., Lippold, G., Adamski, A., and Dyrek, K., *Solid State Ionics* **101–103**, 909 (1997).
8. Grabowski, R., Grzybowska, B., Samson, K., Sloczynski, J., Stoch, J., and Wcislo, K., *Appl. Catal. A* **125**, 129 (1995).
9. Hagen, J., "Industrial Catalysis—A Practical Approach." Wiley–VCH, New York, 1999.
10. Yoon, Y. S., Ueda, W., and Moro-oka, Y., *Catal. Lett.* **35**, 57 (1995).
11. Khodakov, A., Yang, J., Su, S., Iglesia, E., and Bell, A. T., *J. Catal.* **177**, 343 (1998).
12. Khodakov, A., Olthof, B., Bell, A. T., and Iglesia, E., *J. Catal.* **181**, 205 (1999).
13. Chen, K., Xie, S., Iglesia, E., and Bell, A. T., *J. Catal.* **189**, 421 (2000).
14. Barton, D. G., Ph.D. thesis, University of California at Berkeley, 1999.
15. Ressler, T. WinXAS97, version 1.2, 1998.
16. Barton, D. G., Soled, S. L., Meitzner, G. D., Fuentes, G. A., and Iglesia, E., *J. Catal.* **181**, 57 (1999).
17. Liu, Z., and Chen, Y., *J. Catal.* **177**, 314 (1998).
18. Mestl, G., and Srinivasan, T. K. K., *Catal. Rev.—Sci. Eng.* **40**, 451 (1998).
19. Dufresne, P., Payen, E., Grimblot, J., and Bonnelle, J. P., *J. Phys. Chem.* **85**, 2344 (1981).
20. Ohno, T., Miyatu, H., and Kubokawa, Y., *J. Chem. Soc., Faraday Trans.* **83**, 1761 (1987).
21. Mercera, P. D. L., Van Ommen, J. G., Doesburg, E. B. M., Burggraaf, A. J., and Ross, J. R. H., *Appl. Catal.* **57**, 127 (1990).
22. Shadle, E., Hedman, B., Hodgson, K. O., and Solomon, E. I., *Inorg. Chem.* **33**, 4235 (1994).
23. Aritani, H., Tanaka, T., Funabiki, T., Yoshida, S., Kudo, M., and Hasegawa, S., *J. Phys. Chem.* **100**, 5440 (1996).
24. Verbruggen, N. F. D., Mestl, G., von Hippel, L. M. J., Lengeler, B., and Knözinger, H., *Langmuir* **10**, 3063 (1994).
25. Takenaka, S., Tanaka, T., Funabiki, T., and Yoshida, S., *J. Phys. Chem. B* **102**, 2960 (1998).
26. Prinetto, F., Cerrato, G., Ghiotti, G., Chiorino, A., Campa, M. C., Gazzoli, D., and Indovina, V., *J. Phys. Chem.* **99**, 5556 (1995).
27. Afanasiev, P., *Mater. Chem. Phys.* **47**, 231 (1997).
28. Indorina, V., *Catal. Today* **41**, 95 (1998).
29. Chen, K., Khodakov, A., Yang, J., Bell, A. T., and Iglesia, E., *J. Catal.* **186**, 325 (1999).
30. Chen, K., Bell, A. T., and Iglesia, E., *J. Phys. Chem. B* **104**, 1292 (2000).
31. Regalbuto, J. R., and Ha, J. W., *Catal. Lett.* **29**, 189 (1994).
32. Sloczynski, J., Grabowski, R., Wcislo, K., and Grzybowska, B., *Polish J. Chem.* **71**, 1585 (1997).